AD-A185 437 OBSERVATIONS OF ELECTRON CYCLOTRON HARMONIC EMISSIONS ASSOCIATED WITH FIE (U) AEROSPACE CORP EL SEGUNDO CA LAB OPERATIONS H C KOONS ET AL. 01 JUL 87 1/1

UNCLASSIFIED TR-0086(6940-06)-13 SD-TR-87-33 F/G 4/1 NL

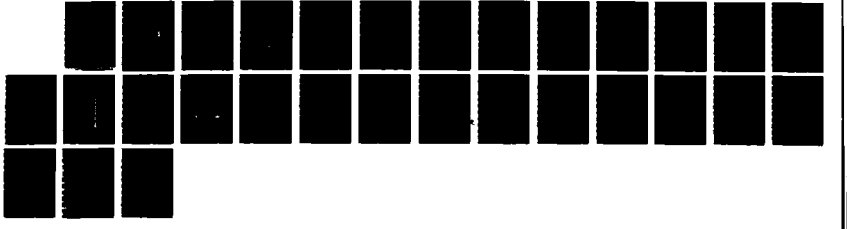

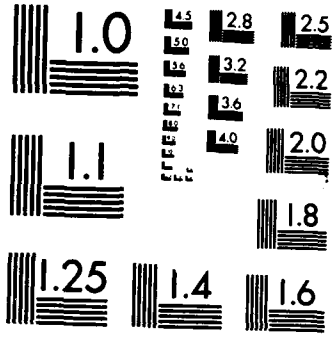

MICROCOPY RESOLUTION TEST CHART
NATIONAL BUREAU OF STANDARDS-1963-A

REPORT SD-TR-87-33

Observations of Electron Cyclotron Harmonic Emissions Associated with Field-Aligned Electron Beams

H. C. KOONS, J. F. FENNELL, and D. J. GORNEY
Space Sciences Laboratory
Laboratory Operations

and

B. C. EDGAR
Space Test Directorate
The Aerospace Corporation
El Segundo, CA 90245

1 July 1987

Prepared for

SPACE DIVISION
AIR FORCE SYSTEMS COMMAND
Los Angeles Air Force Station
P.O. Box 92960, Worldway Postal Center
Los Angeles, CA 90009-2960

6a. NAME OF PERFORMING ORGANIZATION	6b. OFFICE SYMBOL (If applicable)	7a. NAME OF MONITORING ORGANIZATION
Laboratory Operations The Aerospace Corporation		Space Division
6c. ADDRESS (City, State, and ZIP Code)		**7b. ADDRESS (City, State, and ZIP Code)**
El Segundo, CA 90245		Los Angeles Air Force Station Los Angeles, CA 90009-2960
8a. NAME OF FUNDING / SPONSORING ORGANIZATION	**8b. OFFICE SYMBOL (If applicable)**	**9. PROCUREMENT INSTRUMENT IDENTIFICATION NUMBER**
		F04701-85-C-0086
8c. ADDRESS (City, State, and ZIP Code)		**10. SOURCE OF FUNDING NUMBERS**

PROGRAM ELEMENT NO.	PROJECT NO.	TASK NO.	WORK UNIT ACCESSION NO.

11. TITLE (Include Security Classification)
Observations of Electron Cyclotron Harmonic Emissions Associated with Field-Aligned Electron Beams

12. PERSONAL AUTHOR(S)
Koons, Harry C., Edgar, Bruce C., Fennell, Joseph F., and Gorney, David J.

13a. TYPE OF REPORT	13b. TIME COVERED FROM _____ TO _____	14. DATE OF REPORT (Year, Month, Day)	15. PAGE COUNT
		1987 July 1	25

16. SUPPLEMENTARY NOTATION
This work was supported in part by the National Science Foundation under Grant No. ATM-8313655.

17. COSATI CODES			18. SUBJECT TERMS (Continue on reverse if necessary and identify by block number)
FIELD	GROUP	SUB-GROUP	Electron beams Cyclotron harmonic emissions Plasma waves

19. ABSTRACT (Continue on reverse if necessary and identify by block number)

Several cases have been found in plasma wave and electron distribution function data from the SCATHA satellite in which strong gyrofrequency emissions near 1.5 times the local electron gyrofrequency, f_g, correlate in time with field-aligned electron beams. The energy of the electron beams ranges from 100 to 800 eV. Before the beam appears the emissions are observed at a lower frequency, typically 1.1 to 1.2 f_g. As the beam develops, the emissions rise in frequency and grow in amplitude. Above 2 keV the electrons had a normal loss-cone distribution. This loss cone deepened by a small amount when the beams appeared at lower energy. These observations were made near local midnight between L=7.0 and 7.8 R_e.

PREFACE

We gratefully acknowledge valuable discussions with J. Roeder. We are indebted to B. Ledley of the Goddard Space Flight Center for the magnetometer data. We are also indebted to L. Friesen, R. Maulfair, D. Croley and J. Kordan for providing support of the data reduction and analysis.

CONTENTS

FIGURES

I. INTRODUCTION

The study of electrostatic electron cyclotron harmonic (ECH) waves, or $(n + 1/2)f_g$ waves as they are often referred to, in the magnetosphere has recently focused on the source of free energy. Kennel and Ashour-Abdalla[1] have reviewed the basic linear theory for ECH waves in a uniform magnetized plasma. They classify the various instability calculations by their assumed free-energy sources: loss cones, bi-Maxwellian thermal anisotropy, antiloss cones, beams, and anisotropic power-law distributions. There is very little observational support for the plethora of theories on ECH waves. Several papers have associated the observations of ECH waves with the local electron distribution function in order to determine the emission mechanisms and the sources of free energy for these waves. Rönnmark et al.[2] and Kurth et al.[3] reported the appearance of a loss-cone distribution when strong ECH and upper-hybrid emissions were observed. Kurth et al.[4] also observed a positive-sloped perturbation in the perpendicular velocity distribution which appeared during a period when intense ECH waves were also observed. In that case the perturbation in the distribution function was not evident either before or after the waves were observed. Kurth et al.[3] also suggest that a small temperature anisotropy or a small bump in the tail of the perpendicular velocity distribution might be the source of free energy for these waves.

Koons and Fennell[5] have compared wave and particle data from the SCATHA satellite and have found no evidence of the positive slope in the distribution function similar to the one published by Kurth et al.[3] Although the SCATHA particle data show evidence for a loss cone in the plasma sheet, Koons and Fennell also showed that an anti-loss cone or "butterfly" distribution is commonly observed when ECH waves are present. They also showed that strong ECH waves are observed with a variety of spectral forms at the time of a substorm particle injection.

Usually, however, there does not appear to be a one-to-one relationship between the wave spectrum and the electron distribution function. For example, it is not uncommon in the data from the SCATHA satellite to see

significant changes in the wave spectrum with no obvious corresponding change in the particle distribution function and vice versa.

In this report we describe an electron beam velocity distribution that we have been able to associate with intense ECH waves in the magnetosphere. We describe some unique time correlations between changes in the spectrum and intensity of ECH waves and changes in the electron distribution functions measured by the SCATHA satellite.

II. FIELD-ALIGNED ELECTRON BEAMS

Field-aligned electron beams have been a common observation by the particle detectors aboard the SCATHA[6] and ATS 6[7] satellites during geomagnetically disturbed periods. Richardson et al.[6] defined a field-aligned beam as a distribution having a peak in flux at a nonzero energy oriented at approximately 0° or 180° to the magnetic field direction. Their source is unknown. They occur most often in association with substorm injections and almost always are associated with field-aligned ion fluxes. They may be related to the aurora. McIlwain[7] inferred that they were sufficiently intense to cause auroral emissions. Richardson et al.[6] studied the occurrence of field-aligned electron beams in the SCATHA data from 1979 and found that the highest number of beam observations occurred for low electron energies between 32 and 64 eV. The distribution of beam energies ranged from 16 eV to 1 keV, and the electron beams were always counterstreaming or bidirectional (peaked at 0 deg and 180 deg to the magnetic field line). McIlwain[7] noted that the more energetic beams (i.e., those above 1 keV) seemed to occur only within the first minutes after a substorm associated with a plasma injection. During the period of the observations we report here from May 1979, the particle detectors on the SCATHA instrument were limited to 87 eV as the lowest energy channel.

Bernstein et al.[8] reported a laboratory experiment in which a monoenergetic field-aligned electron beam between 50 eV and 50 keV generated ECH waves. An important aspect of Bernstein et al.'s experimental results was the association of ECH waves with a counterstreaming electron beam configuration parallel to the magnetic field. A unidirectional beam only produced weak emissions at the electron plasma frequency.

III. EXPERIMENT DESCRIPTION

In the following sections we present examples of simultaneous wave and particle data measured by the SCATHA satellite in May 1979. The complement of scientific instruments is described by Fennell.[9] The spacecraft orbit is equatorial with a 23 hour 35 min period, a 7.9-deg inclination, a 7.78-R_e apogee, and a 5.32-R_e perigee. The spin period of the satellite is 60 s. The data presented in this report were obtained at relatively low magnetic latitudes, within two hours of local midnight and near SCATHA's apogee.

The VLF receiver detects the broadband spectrum from 100 Hz to 5 kHz.[10] The antenna is a 100-m tip-to-tip electric dipole provided by the Goddard Space Flight Center. The receiver covers a dynamic range of 80 dB with automatic gain control (AGC). The analog data are spectrum analyzed in the laboratory using a Sanders Spectrum Analyzer. The narrowband VLF data used in this report were obtained from three frequency channels at 1.3, 2.3, and 3.0 kHz (± 7.5% bandwidth). The particle distribution functions were obtained from the Aerospace electrostatic analyzers covering the energy range from 87 eV to 20 keV.[9] The values for the electron gyrofrequency were computed from the local magnetic field measured by the onboard flux-gate magnetometer provided by the Goddard Space Flight Center.

IV. WAVE OBSERVATIONS

On two days during May 1979 very intense ECH waves were detected by the VLF receiver aboard SCATHA. Figure 1 shows the distribution of the peak amplitudes of ECH waves observed during broadband analog data acquisitions from April to November 1979. To obtain these peak amplitudes, data from the narrow band channels were averaged over 16 s periods during times when ECH waves were observed. The ECH waves were identified from their characteristic appearance and frequency range in the broadband spectrograms. This limited the study to the times of the broadband data acquisitions, which were typically two hours per day and uniformly spaced in local time. The emissions with the two highest amplitudes occurred at 0010 UT on May 20 and at 2258 UT on May 28.

The auroral index (AE) indicates that a large substorm was observed by several ground stations near 2100 UT on May 19 and that the level of activity remained relatively high throughout the early hours of May 20. On May 28 near 2200 UT the auroral index indicates a small substorm occurred near the longitude of the SCATHA satellite. The substorm was very local because it was observed at only a few ground stations.

The dynamic spectrum (bottom panel) and the wave amplitude in the 2.3 kHz channel (top panel) for the time period from 0002 to 0014 UT on May 20, 1979 are shown in Figure 2. These data were obtained near 0100 local time. The wave amplitude plotted in the top panel is a 16 s average of the electric field strength. The bottom panel shows the wave spectrum at frequencies up to 3 kHz. The thin essentially horizontal lines on the spectrogram are drawn at 1, 1.1, 1.2, 1.3, 1.4 and 1.5 f_g (based on the magnetic field measurements that were sampled every 0.25 s). The small variations in the gyrofrequency during this time indicate that the local magnetic field was only slightly disturbed. The waves below f_g are electromagnetic chorus emissions characterized by a gap in the frequency spectrum at one-half of the electron gyrofrequency.[11,12] The electron cyclotron harmonic waves occur above the electron gyrofrequency. On two occasions during the time period shown in the spectrogram the ECH from f_g to 2 f_g increased from a frequency low in the band

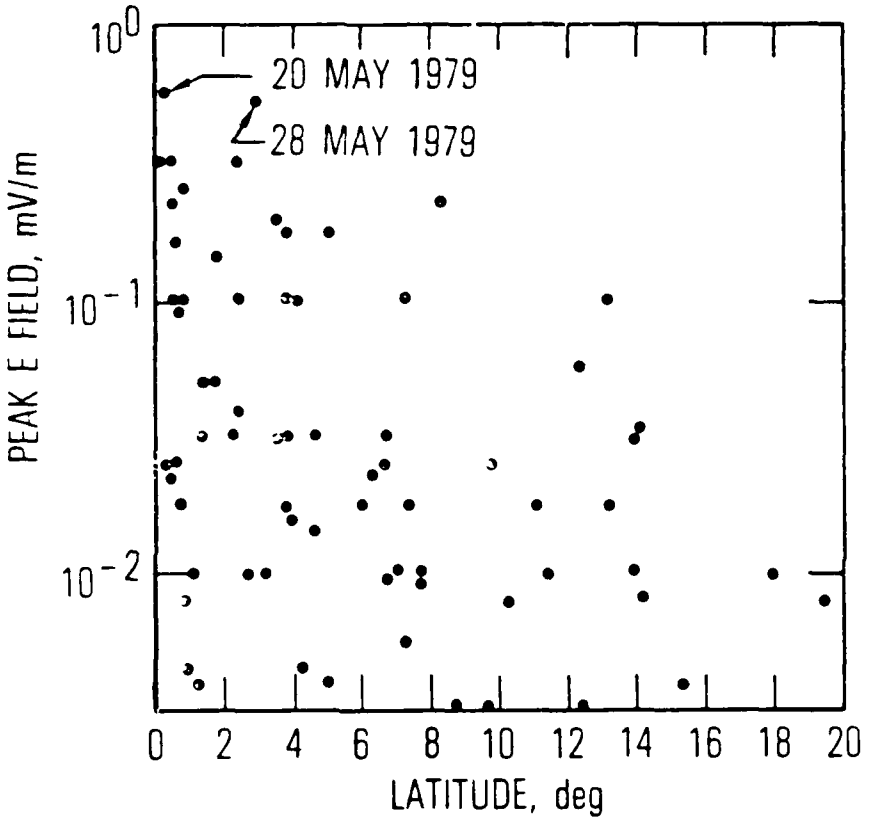

Fig. 1. The amplitude distribution for the maximum electric field observed in either the 1.3 or 2.3 kHz channel by the VLF receiver aboard the SCATHA satellite for electrostatic electron cyclotron harmonic waves observed during each acquisition of broadband VLF data between April and November 1979.

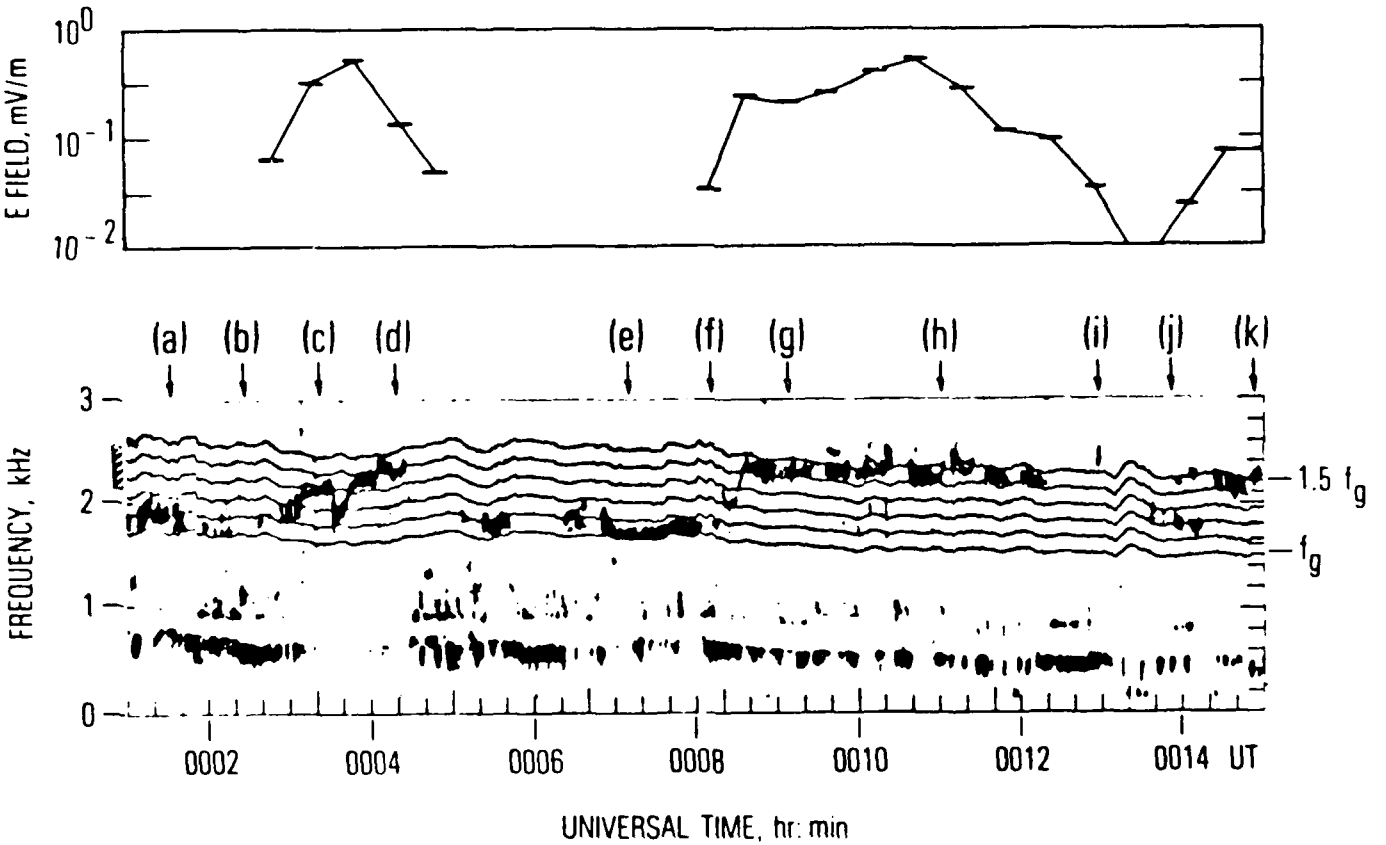

Fig. 2. Wave amplitude (top) in the 2.3 kHz narrowband channel, and spectrogram (bottom) of VLF emissions detected on May 20, 1979. The thin horizontal lines are drawn at 1, 1.1, 1.2, 1.3, 1.4, and 1.5 times the electron gyrofrequency. The cross-hatched area on the left of the spectrogram shows the bandwidth of the 2.3 kHz channel.

between f_g and 1.1 f_g to a frequency in the middle of the band between 1.4 and 1.5 f_g. The first time occurred in the interval from 0003 to 0004 UT. The frequencies then decreased to the low end of the band by 0005 UT. From 0005 to 0008 UT the waves remain near the electron gyrofrequency. Again at about 0008:30 UT the frequency rapidly increased to the middle of the band and stayed there for several minutes. During the time intervals when the waves are observed near 1.5 f_g their amplitude reached its maximum value of about 0.6 mV/m in the 2.3-kHz channel.

The dynamic spectrum (bottom panel) and the wave amplitudes in the 1.3-kHz channel (top panel) for the second time period from 2240 to 2300 UT on May 28, 1979 are shown in Figure 3. Two time periods on this spectrogram are noteworthy: first, at 2244 UT when waves appeared up to the fifth harmonic band for a short interval and second at 2258 UT when waves again appeared up to the fourth harmonic band. In each instance the wave amplitude greatly increased. The frequency shift of the waves at 2258 UT was very similar to the frequency shift observed on May 20. Before and after the appearance of the harmonics the waves in the lowest band were near 1.1 f_g. While the harmonics were present the waves were centered about a frequency slightly above 1.5 f_g. Note also that the higher "harmonics" are not integer multiples of 1.5 f_g but are in fact 2.3, 3.2, and 4.0 f_g. The peak wave amplitudes on May 28 were only slightly lower than the wave amplitudes measured on May 20.

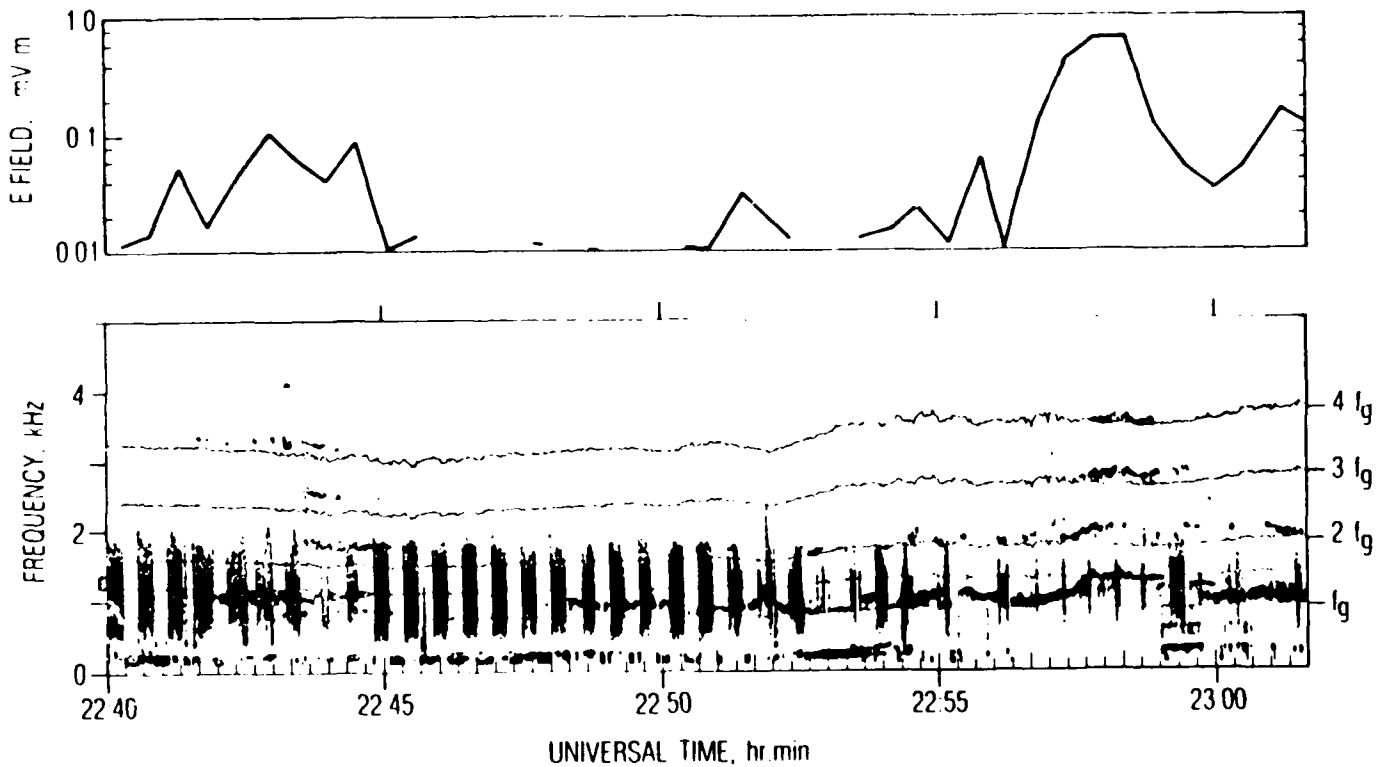

Fig. 3. Wave amplitude (top) in the 1.3 and 3.0 kHz narrowband channels, and spectrogram (bottom) of VLF emissions detected on May 28, 1979. The thin horizontal lines are drawn at 1, 1.5, 2, 3, and 4 times the electron gyrofrequency. The cross-hatched area on the left of the spectrogram shows the bandwidth of the 1.3 kHz channel.

V. ELECTRON OBSERVATIONS

Figures 4 and 7 show examples of the velocity space distribution functions for the electrons from time periods of interest on May 20 and 28 when the intense ECH waves were observed. A distinct feature of these distribution functions is the presence of relatively low energy electron beams during the time periods when the ECH waves are most intense and occurring at the middle of the first harmonic band.

Figure 4 covers the time period from 0001:48 to 0004:40 UT on May 20. Each distribution function is obtained over one spin period (one minute) of the satellite. The maximum wave intensity occurs in conjunction with the distribution function shown in Fig. 4c. The obvious change that has appeared in the progression from the distribution function at 0001:48 (Fig. 4a) to the one at 0003:42 (Fig. 4c) is the elongated feature parallel to the magnetic field at velocities below 2×10^4 km/s (< 1 keV). In this representation there appears to be little change in the distribution function at higher velocities.

The electron temperature (i.e., the average energy) parallel and perpendicular to the direction of the magnetic field has been calculated from the particle measurements and the anisotropy of the distribution function, $(T_\perp - T_\parallel)/T_\parallel$, determined by Kennel and Petschek.[13] The anisotropy is shown in Fig. 5 as a function of time for the period of interest on May 20. The anisotropy actually decreased during the time period near 0003 UT when the waves intensified. This occurred because the perpendicular temperature decreased while the parallel temperature increased. We have found that a graph of the actual electron fluxes as a function of time for each of the energy channels gives a better picture of the changes in the distribution function than do the moments of the distribution function such as the temperature. The fluxes for the lower energy channels are shown in Fig. 6 for pitch angles nearly parallel (0 to 20 deg and 160 to 180 deg) and nearly perpendicular (70 to 110 deg) to the magnetic field. The increase in the fluxes parallel (solid line in the figure) to the magnetic field is very apparent

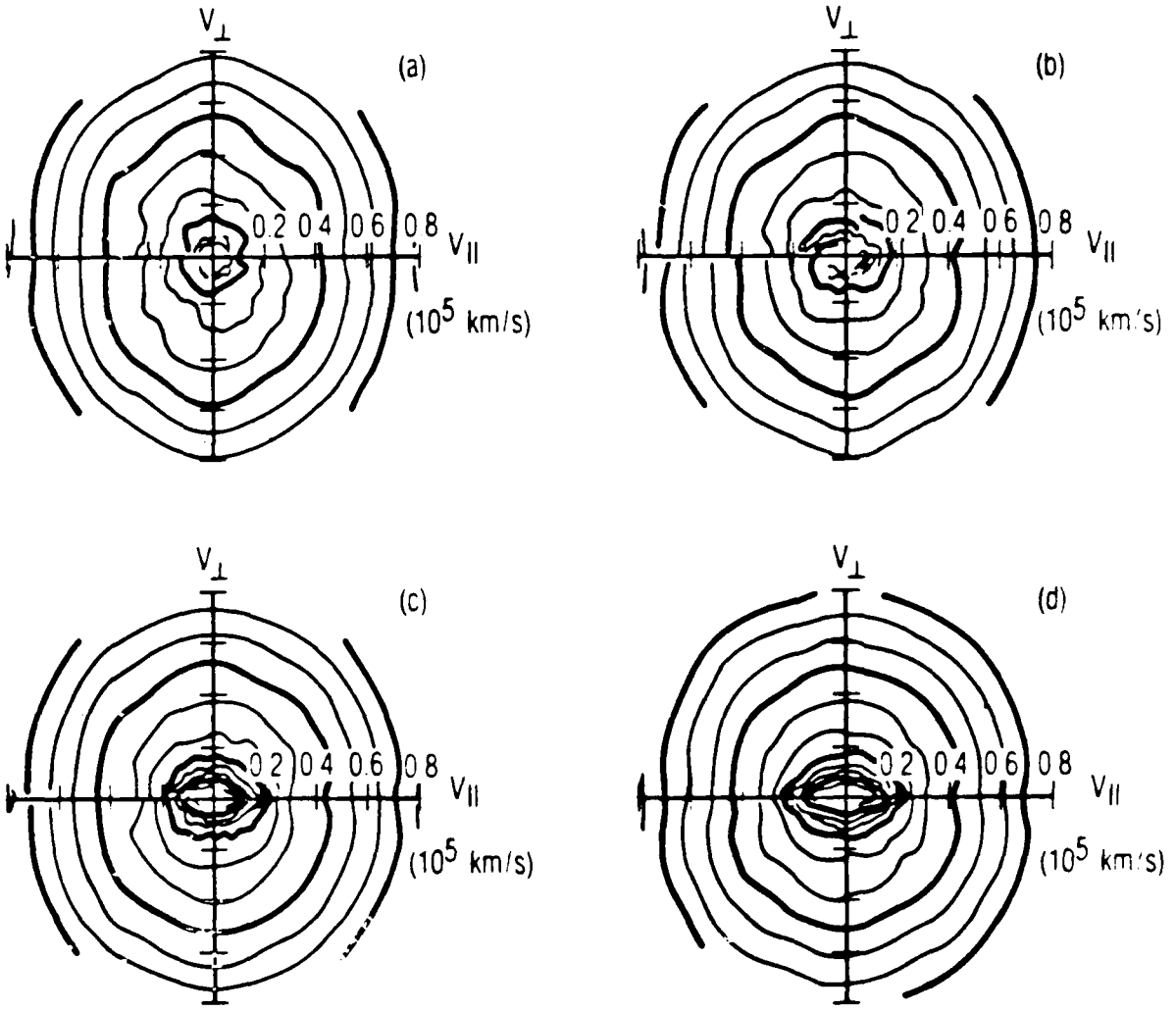

Fig. 4. Electron distribution functions for the first electron cyclotron wave enhancement on May 20, 1979. (a) 0002 UT, (b) 0003 UT, (c) 0004 UT, (d) 0005 UT. The horizontal axis is the velocity parallel to the magnetic field. The heavy contours indicate orders of magnitude in f(v), with maximum f(v) toward the origin in v. The outermost heavy contour corresponds to a phase space density of 2.5×10^{-2} km^{-6} sec^{3}.

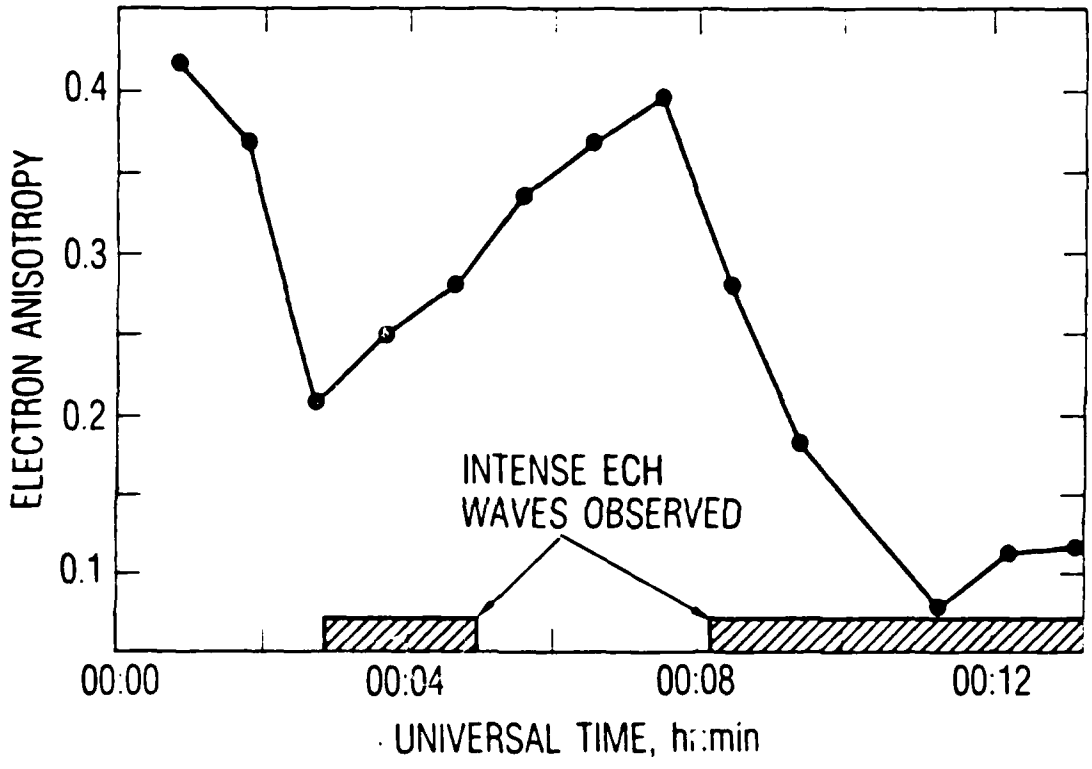

Fig. 5. The anisotropy of the electron distribution function, $(T_\perp - T_\parallel)/T_\parallel$, as a function of time during the ECH wave enhancements on May 20, 1979. The two time periods when intense waves were observed are marked on the figure.

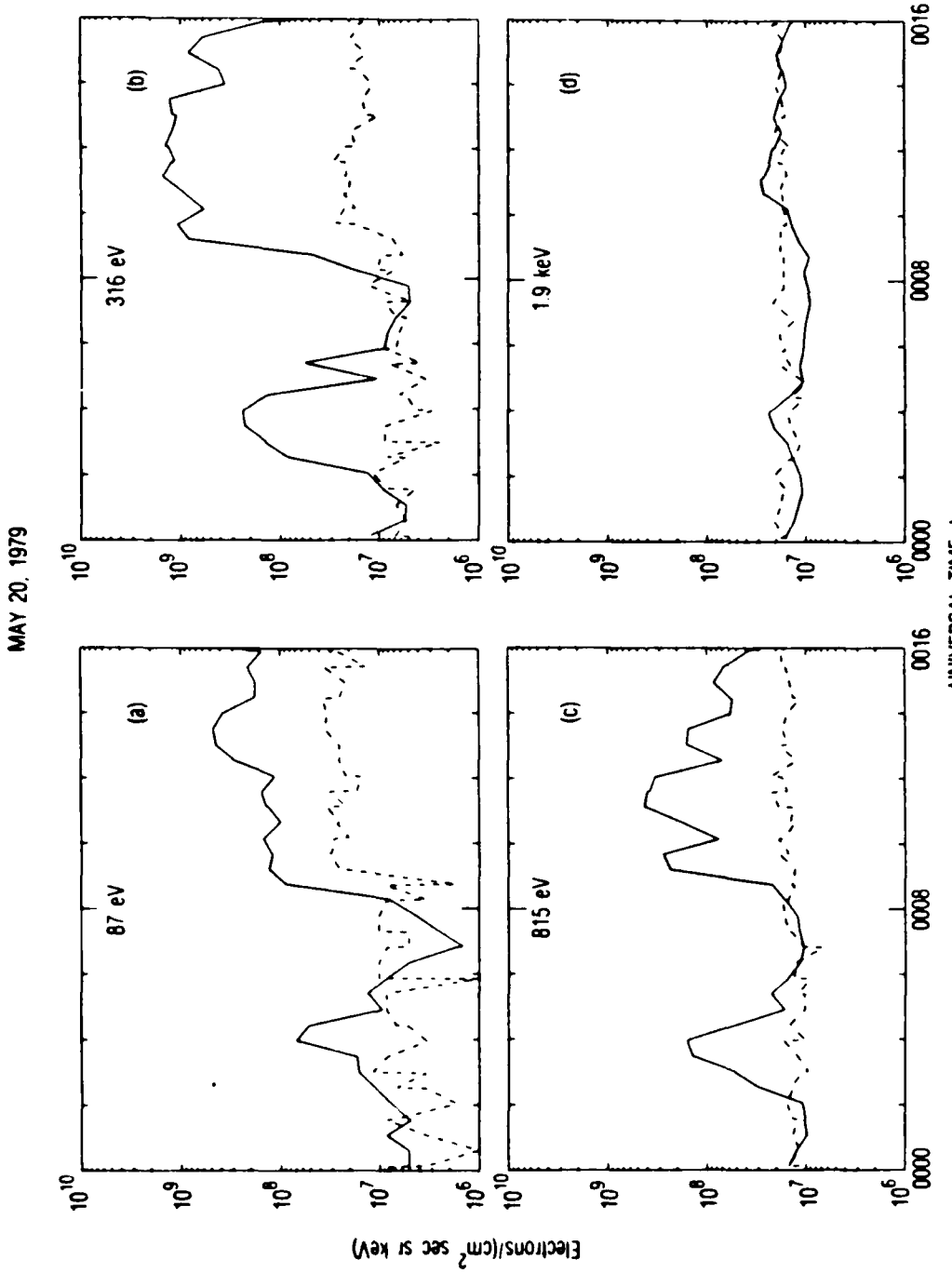

Fig. 6. Electron fluxes parallel (solid line) and perpendicular (dashed line) to the magnetic field as a function of time on May 20, 1979. (a) 87 eV, (b) 316 eV, (c) 815 eV, and (d) 1.94 keV.

just after 0003 UT. At low energies this distribution is an electron beam of the type described by Richardson et al.[6]

The distribution functions for the time period from 0007:32 to 0011:21 on May 20, which includes the second time period on May 20 when the intense ECH waves were observed, were essentially identical to those in Fig. 4. At the beginning the distribution at the lower energies (< 1 keV) was generally isotropic while at higher energies it was a normal "loss cone" or "pancake" distribution. The waves at this early time are observed between 1.0 and 1.1 f_g. During the next three minutes a low-energy electron beam forms (see Fig. 6). This is accompanied by a decrease in the electron temperature (i.e., the spectrum softens) both parallel and perpendicular to the magnetic field. Again the temperature anisotropy decreases because the perpendicular temperature decreased more than the parallel temperature. The formation of the electron beam corresponded to the intensification of the ECH waves and the increase in their frequency to approximately 1.5 f_g. The fluxes shown in Fig. 6 show more than an order of magnitude increase parallel to the magnetic field for energies at and below 1 keV. There is little change in the fluxes above ~ 2 keV.

The wave data (Fig. 2) show a clear correlation of the frequency shift of the waves from 1.1 to 1.5 f_g with the change in the electron distribution function from an essentially isotropic distribution to a field-aligned beam distribution (Fig. 4). The correlation of the wave amplitude with the beam is less certain. Since the amplitude is only measured in the 15% pass band at 2.3 kHz, the signal at 1.5 f_g would be measured to be stronger than the comparable signal at 1.1 f_g because the former is better centered within the pass band of the amplitude measurement.

The low velocity region of selected electron distribution functions from May 28 are shown in Fig. 7 to highlight the field-aligned nature of the low-energy electrons. The sequence of changes in the distribution function during the two wave enhancements on May 28 closely follows the sequence on May 20 shown in Fig. 4. The distribution function in Fig. 7a was observed when the ECH emissions were weak and centered near 1.1 f_g. The distribution in Fig. 7b

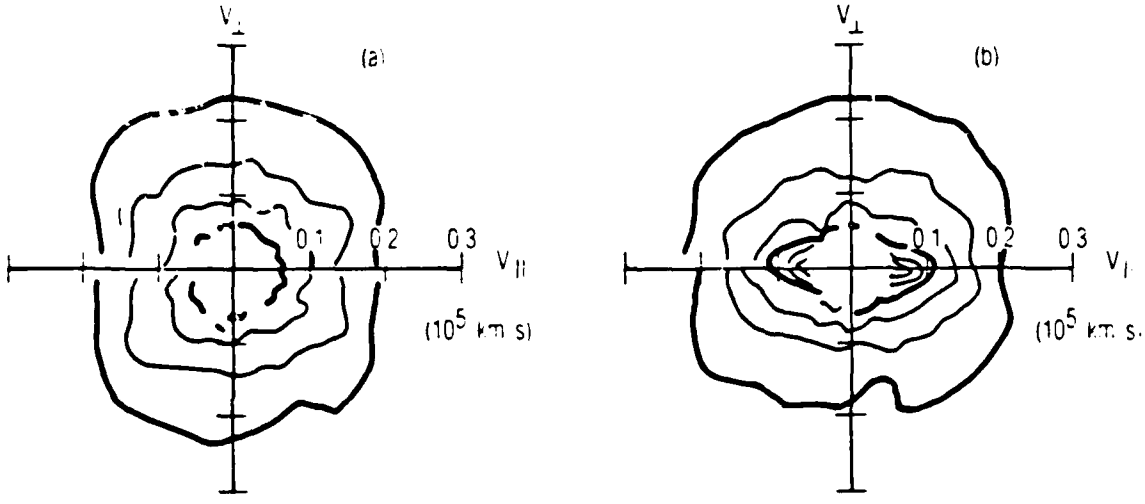

Fig. 7. The low-velocity portion of the electron distribution functions for the second electron cyclotron wave enhancement on May 28, 1979 -- (a) prior to the enhancement at 2253 UT, and (b) during the enhancement at 2258 UT. The horizontal axis is the velocity parallel to the magnetic field. The heavy contours indicate orders of magnitude in f(v), with maximum f(v) near the origin in v. The outermost heavy contour corresponds to a phase space density of 2.5 km^{-6} sec^3.

was observed when the ECH emissions were strong and centered near 1.5 f_g. The electron temperature displayed more rapid variation during this time period than it did on May 20. The parallel and perpendicular temperatures change together, resulting in little change in the temperature anisotropy. The fluxes plotted in Fig. 8 show that during the first intensification of the wave amplitude on May 28 there was a gradual increase in the ratio of the fluxes parallel/perpendicular to the magnetic field. A close scrutiny of the distribution functions showed that a field-aligned structure formed in the electron distribution function at that time at the lowest velocities measured. The data in Fig. 8 show that the parallel flux increased from 2230 to 2245 UT relative to the perpendicular flux. Not only is the field alignment tighter but the parallel flux is higher. That increase in the parallel flux gives the appearance of a beam in the distribution functions. Technically it is not a beam within the energy range of the instrument according to the standard definition because the flux decreases monotonically from 87 eV toward higher energy.

The second enhancement in the wave intensity on May 28 occurs at about 2258 UT. The distribution function for that time is shown in Fig. 7b. Again there was a noticeable elongation at lower velocities along the parallel velocity axis. This feature stands out quite well in the fluxes plotted in Fig. 8. During the period from 2257 to 2300 UT the field-aligned electron distribution was observed to evolve such that there was a growth of the particle beam in the direction parallel to the magnetic field before the appearance of the beam in the direction antiparallel to the magnetic field. This could be either a temporal or a spatial effect. With the present data set we cannot distinguish the two possibilities.

The field-aligned nature of the electrons is brought out more strongly by examining the pitch-angle distributions of the individual electron energy channels. The circles in Figure 9 show the measured fluxes for the electrons as a function of pitch angle during a 200-s time period from 2256:40 to 2300:00 UT on May 28. This is a period of intense wave activity. The bottom panel in the figure shows the strong field-aligned structure in the low-energy electrons (187 eV channel). The upper panel shows the loss cone in the

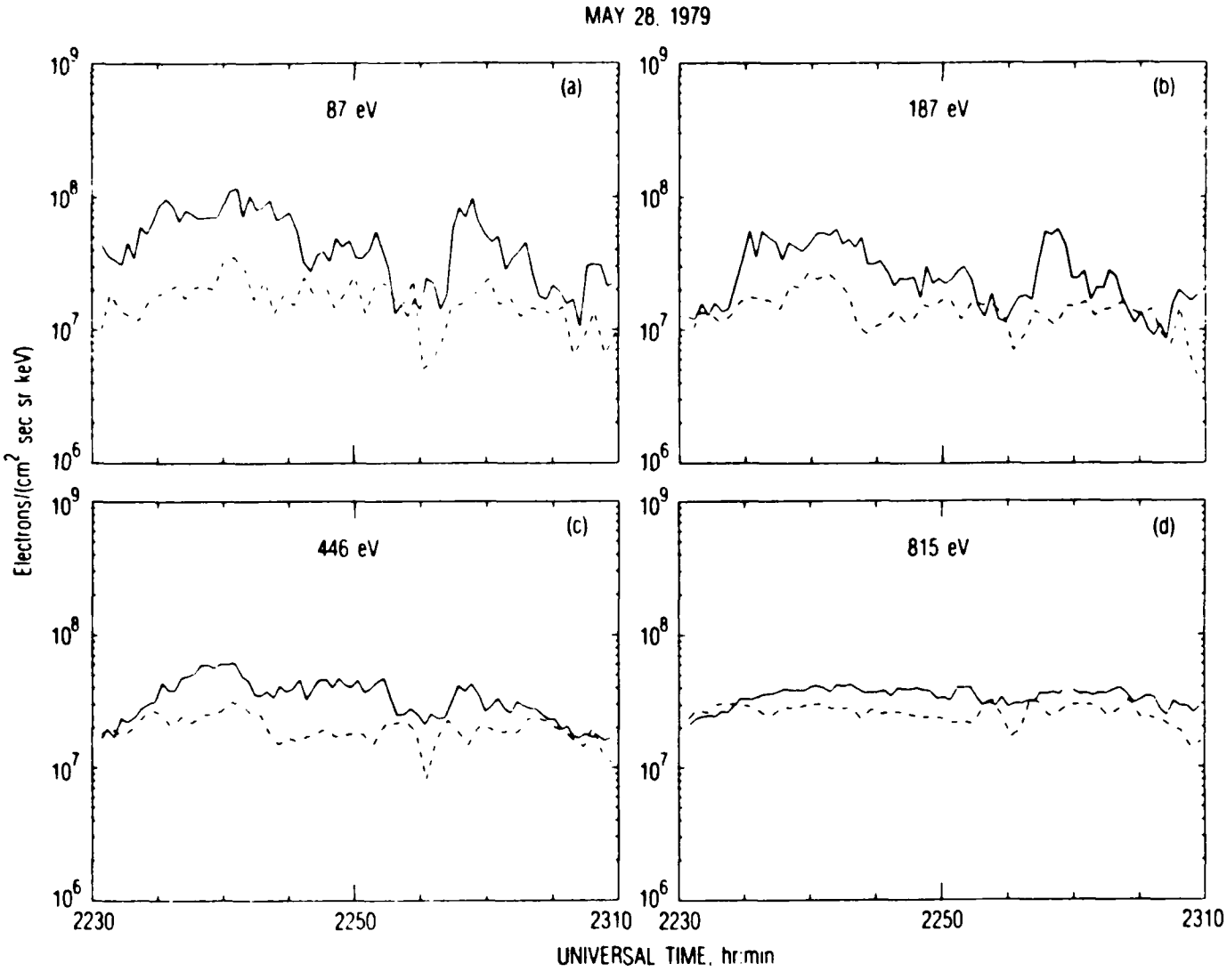

Fig. 8. Electron fluxes parallel (solid line) and perpendicular (dashed) to the magnetic field as a function of time on May 28, 1979. (a) 87 eV, (b) 187 eV, (c) 446 eV, and (d) 815 eV.

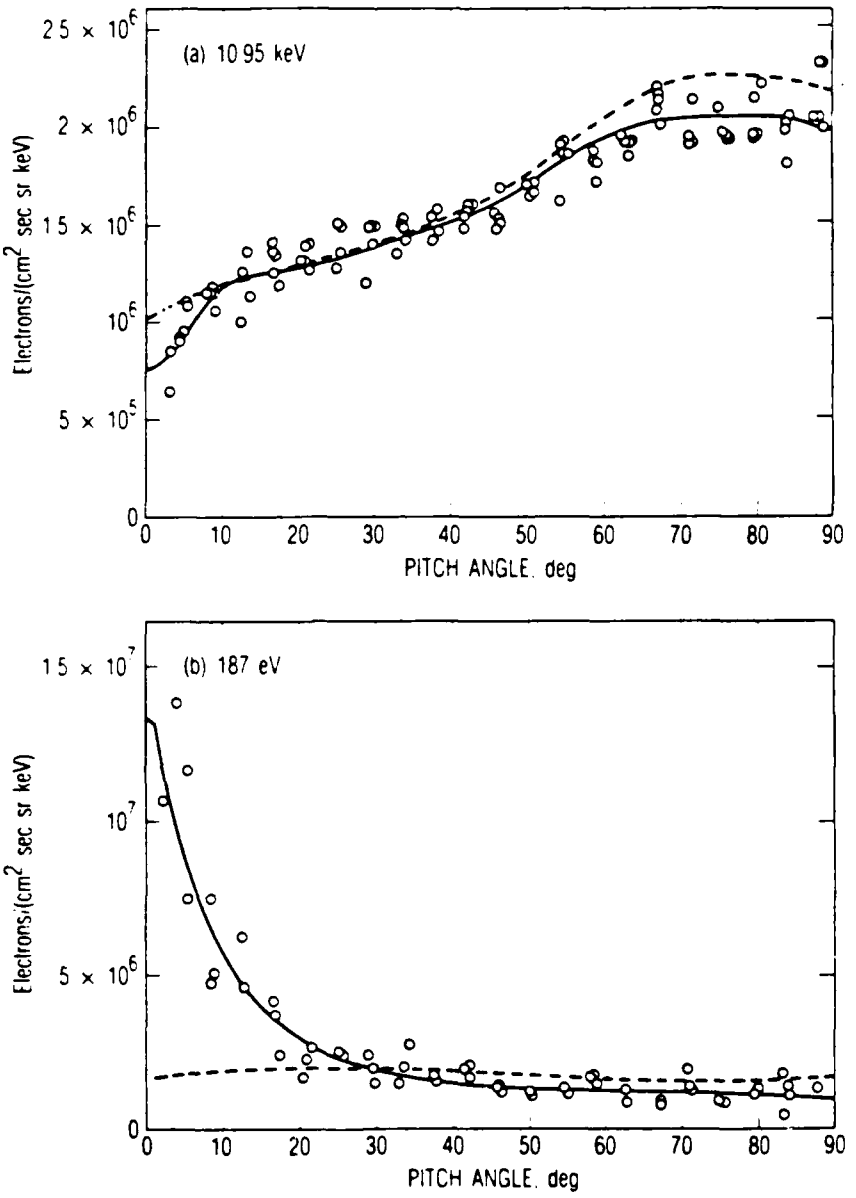

Fig. 9. Measured electron fluxes (circles) as a function of pitch angle for a period of intense wave activity between 2256:40 and 2300:00 UT on May 28, 1979 at 187 eV (bottom panel) and 10.95 keV (top panel). Pitch-angle distribution (solid line) determined from the measurements shown as circles, using a maximum entropy technique for determining the true distribution from the observations and the angular response of the instrument. Pitch-angle distribution shown for comparison for a period of weak wave activity between 2250:00 and 2253:20 UT on May 28 (dashed line), determined from measurements not shown on the figure using a maximum entropy technique.

higher-energy electrons (10.95 keV channel). The solid curve in each panel is the angular distribution determined by unfolding the instrumental response function using a maximum entropy technique.[14] The dashed curve in each panel shows the angular distribution obtained from the maximum entropy technique during the 200-s time period from 2250:00 to 2253:20 UT. That was a time period with low wave amplitudes. At that time there is no evidence for a field-aligned distribution at low energies and a significantly smaller loss cone at higher energies. There is also an enhancement in the number of locally mirroring particles near 90 deg.

VI. SUMMARY

The most intense electron cyclotron harmonic waves detected by the VLF receiver aboard the SCATHA satellite were accompanied by an elongation of the electron distribution function along the parallel velocity axis. This elongation formed a beam on May 20 and a field-aligned structure on May 28. This change in the distribution function was limited to energies below 2 keV and was most apparent at energies below 1 keV. This is the best correlation between waves and particles that has been found to date in the analysis of the data from the SCATHA satellite.

The energy of the electrons in the beam that we have associated with the ECH waves is consistent with the energy of the electrons in the beams described by McIlwain,[7] who states that field-aligned electron distributions were very rare for energies greater than 2 keV.

Since there is little change in the electron distribution function above 2 keV, there is no direct evidence that the electrons above 2 keV interact with these waves even though they are the most intense waves measured during the eight-month period covered by the analysis. However, to obtain positive growth a region of positive slope is required somewhere in the distribution function.[1] In the observed distributions this only appears in the loss cone at energies above 2 keV. This suggests that the waves are actually generated by the electrons above 2 keV and that the role of the low-energy electron beam is to change the dispersion characteristics of the waves, resulting in the observed changes in frequency and amplitude. We note in Fig. 9 that the loss cone at the higher energy deepened by a small amount at the same time that the electron beam appeared.

REFERENCES

1. Kennel, C. F., and M. Ashour-Abdalla, Electrostatic Waves and the Strong Diffusion of Magnetospheric Electrons, in Magnetospheric Plasma Physics, ed. A. Nishida, D. Reidel, Boston, MA, 1982.

2. Ronnmark, K., H. Borg, P. J. Christiansen, M. P. Gough, and D. Jones, Banded electron cyclotron harmonic instability - A first comparison of theory and experiment, Space Sci. Rev., 22, 401, 1978.

3. Kurth, W. S., J. D. Craven, L. A. Frank and D. A. Gurnett, Intense electrostatic waves near the upper hybrid resonance frequency, J. Geophys. Res., 84, 4145, 1979.

4. Kurth, W. S., L. A. Frank, M. Ashour-Abdalla, D. A. Gurnett and B. G. Burek, Observations of a free-energy source for intense electrostatic waves, Geophys. Res. Lett., 7, 293, 1980.

5. Koons, H. C., and J. F. Fennell, Particle and waves dynamics during plasma injections, J. Geophys. Res., 88, 6221, 1983.

6. Richardson, J. D., J. F. Fennell, and D. R. Croley, Jr., Observations of field-aligned ion and electron beams from SCATHA (P78-2), J. Geophys. Res., 86, 10105, 1981.

7. McIlwain, C. E., Auroral electron beams near the magnetic equator, in Physics of the Hot Plasma in the Magnetosphere, ed. B. Hultquist and L. Stenflo, p. 91, Plenum, NY, 1975.

8. Bernstein, W. H., H. Leinbach, H. Cohen, D. S. Wilson, T. N. Davis, T. Hallinan, B. Boker, J. Martz, R. Zeimke, and W. Huber, Laboratory observations of RF emissions at ω_{pe} and $(n + 1/2)\ \omega_{ce}$ in electron beam-plasma and beam-beam interactions, J. Geophys. Res., 80, 4375, 1975.

9. Fennell, J. F., Description of P78-2 (SCATHA) satellite and experiments, The IMS Source Book, Russell and Southwood, eds., p. 65, Am. Geophys. Union, Washington, DC, 1982.

10. Koons, H. C., Role of hiss in magnetospheric chorus emissions, J. Geophys. Res., 86, 6745, 1981.

11. Tsurutani, B. T., and E. J. Smith, Postmidnight chorus: A substorm phenomenon, J. Geophys. Res., 79, 118, 1974.

12. Burtis, W. J., and R. A. Helliwell, Magnetospheric chorus: Occurrence patterns and normalized frequency, Planet. Space Sci., 24, 1007, 1976.

13. Kennel, C. F., and H. E. Petschek, Limit on stably trapped particle fluxes, J. Geophys. Res., 71, 1, 1966.

14. Gorney, D. J., and J. L. Roeder, Restoration of charged-particle pitch-angle distribution measurements using a maximum entropy algorithm, Trans. Am. Geophys. Union (EOS), 1986.

LABORATORY OPERATIONS

The Aerospace Corporation functions as an "architect-engineer" for national security projects, specializing in advanced military space systems. Providing research support, the corporation's Laboratory Operations conducts experimental and theoretical investigations that focus on the application of scientific and technical advances to such systems. Vital to the success of these investigations is the technical staff's wide-ranging expertise and its ability to stay current with new developments. This expertise is enhanced by a research program aimed at dealing with the many problems associated with rapidly evolving space systems. Contributing their capabilities to the research effort are these individual laboratories:

Aerophysics Laboratory: Launch vehicle and reentry fluid mechanics, heat transfer and flight dynamics; chemical and electric propulsion, propellant chemistry, chemical dynamics, environmental chemistry, trace detection; spacecraft structural mechanics, contamination, thermal and structural control; high temperature thermomechanics, gas kinetics and radiation; cw and pulsed chemical and excimer laser development including chemical kinetics, spectroscopy, optical resonators, beam control, atmospheric propagation, laser effects and countermeasures.

Chemistry and Physics Laboratory: Atmospheric chemical reactions, atmospheric optics, light scattering, state-specific chemical reactions and radiative signatures of missile plumes, sensor out-of-field-of-view rejection, applied laser spectroscopy, laser chemistry, laser optoelectronics, solar cell physics, battery electrochemistry, space vacuum and radiation effects on materials, lubrication and surface phenomena, thermionic emission, photosensitive materials and detectors, atomic frequency standards, and environmental chemistry.

Computer Science Laboratory: Program verification, program translation, performance-sensitive system design, distributed architectures for spaceborne computers, fault-tolerant computer systems, artificial intelligence, microelectronics applications, communication protocols, and computer security.

Electronics Research Laboratory: Microelectronics, solid-state device physics, compound semiconductors, radiation hardening; electro-optics, quantum electronics, solid-state lasers, optical propagation and communications; microwave semiconductor devices, microwave/millimeter wave measurements, diagnostics and radiometry, microwave/millimeter wave thermionic devices; atomic time and frequency standards; antennas, rf systems, electromagnetic propagation phenomena, space communication systems.

Materials Sciences Laboratory: Development of new materials: metals, alloys, ceramics, polymers and their composites, and new forms of carbon; nondestructive evaluation, component failure analysis and reliability; fracture mechanics and stress corrosion; analysis and evaluation of materials at cryogenic and elevated temperatures as well as in space and enemy-induced environments.

Space Sciences Laboratory: Magnetospheric, auroral and cosmic ray physics, wave-particle interactions, magnetospheric plasma waves; atmospheric and ionospheric physics, density and composition of the upper atmosphere, remote sensing using atmospheric radiation; solar physics, infrared astronomy, infrared signature analysis; effects of solar activity, magnetic storms and nuclear explosions on the earth's atmosphere, ionosphere and magnetosphere; effects of electromagnetic and particulate radiations on space systems; space instrumentation.

END

11-87

DTIC